

Near-infrared speckle imaging and AO polarimetry of the bipolar proto-planetary nebula Frosty Leo



K. Murakawa ⁽¹⁾, K. Ohnaka ⁽¹⁾, T. Driebe ⁽¹⁾, K.-H. Hofmann ⁽¹⁾, D. Schertl ⁽¹⁾,
S. Oya ⁽²⁾, and G. Weigelt ⁽¹⁾



(1) Max-Planck-Institut für Radioastronomie, Bonn, Germany

(2) Subaru Telescope, National Astronomical Observatory of Japan, Hawaii, USA

Introduction

IRAS 09371+1212 is an oxygen-rich post-asymptotic giant branch (post-AGB) star with an hourglass-like bipolar proto-planetary nebula (PPN), and has been well studied since its discovery because of several interesting peculiarities. It is also known as Frosty Leo because its unique, strong peak at $60 \mu\text{m}$ in the IRAS photometry was initially proposed to be due to emissions from water ice which condensed onto dust grains in the circumstellar envelope (Forveille *et al.* 1987). Rouan *et al.* (1988) identified the absorption feature attributed to water ice at $3.1 \mu\text{m}$ and found the optical depth $\tau_{3.1\mu\text{m}}$ of ~ 3.3 . This value is comparable to that of the PPN OH 231.8+4.2 ($\tau \sim 2.5$, Smith *et al.* 1988), but exceptionally larger than other oxygen-rich evolved stars (Meyer *et al.* 1998).

The distinct bipolarity is remarkable. Rouan *et al.* (1988) first resolved the two bipolar lobes toward the south and north with a $2''.4$ separation in the *JHKL* bands with the 3.6 m CFH telescope. Adaptive optics imaging detected the bright central star (Beuzit *et al.* 1994; Roddier *et al.* 1995). Dougados *et al.* (1990) and Scarrott & Scarrott (1990) performed imaging polarimetry in the *JK* bands and *BVRI* bands, respectively. The polarimetric data showed a centrosymmetric vector pattern in the bipolar lobes and a so-called polarization disk between them. This polarization signature implies the presence of an enhanced equatorial dust concentration seen edge-on. While it has an axisymmetric appearance $< 5''$ from the central star, several complex structures such as ansae and jets have been detected (Sahai *et al.* 2000).

It is thought that the formation of a bipolar nebula requires the factor of additional effects besides the superwind and the interacting stellar wind (Kwok 1993). Widely accepted interpretations argue that the most possible mechanism is interaction with binary companions (e.g. Balick & Frank 2002). High-resolution imaging and polarimetry with radiative transfer modeling is an important approach to provide us unique science results and a better understanding of when and how the mechanism works to shape the circumstellar dust shell.

Observations

The *K*-band speckle imaging of Frosty Leo were performed using the 6 m SAO telescope on March 11, 2001. The resulting image (Fig. 1 top-left) was reconstructed from the 581 speckle interferograms by means of the speckle masking bispectrum method (Weigelt 1977; Lohmann *et al.* 1983).

Near-infrared imaging polarimetry is a powerful technique to extract important information of dust shell structures, which are hard to be detected from the total intensity images (e.g. Murakawa *et al.* 2005). *HK* band polarimetric images were obtained using the high-resolution near-infrared camera CIAO with 36 element adaptive optics on the 8 m Subaru telescope on January 10, 2004. A turnable half-wave plate and a wire-grid polarizer allowed us to measure linear polarization. The Stokes *QUV* parameter images, the degree of linear polarization images, and the orientation of the polarization were derived from the observed data (Fig. 1 middle and bottom). Our high-resolution images show:

- An hourglass-like bipolarity: bipolar lobes extending toward the south and the north with $\sim 3''$ extension, an equatorial narrow waist at a position angle of 75° , and a spherical feature of the bright central star.
- A point-symmetric appearance with clumpy structures in the bipolar lobes.
- A centrosymmetric polarization vector pattern in the bipolar lobes and a polarization disk between them.
- An elongated region with small polarizations lying at a position angle of -45° .
- Polarization vectors in the polarization disk at the east side of the central star are potentially aligned along the disk plane.

Radiative transfer modeling

We have performed radiative transfer calculations to model the circumstellar dust shell of Frosty Leo. We attempted, for the first time, to reproduce the spectral energy distribution (SED) curve, the total intensity images and the polarization maps with a single model of this object. Polarization analysis is a powerful technique to derive the properties and distribution of dust.

We used a recently developed radiative transfer code, which simulates scattering and thermal emission of radiation by spherical dust grains in a three-dimensional model geometry by means of the Monte Carlo method (Ohnaka *et al.* 2006). This code computes the SEDs, the dust temperature distribution and the Stokes *QUV* parameters. We modified the original code to use the method proposed by Fischer *et al.* (1994) to determine the direction of the scattered light. This algorithm takes into account the polarization status of the incident light; therefore, it provides a better solution, in particular in cases where there is a large number of scattering times or a highly polarized light.

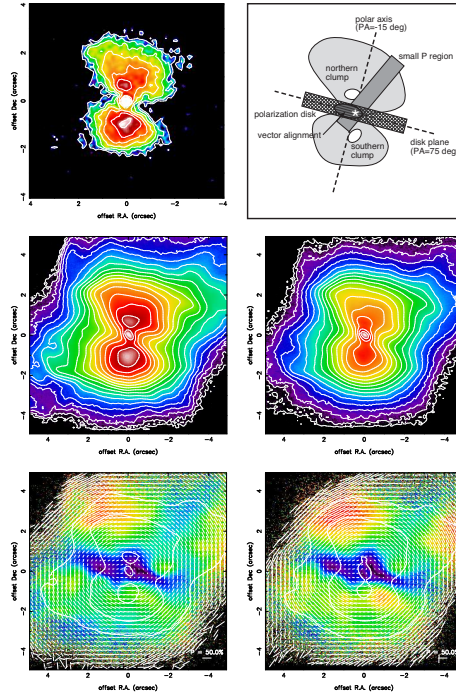


Figure 1: top-left: Our *K* band speckle image with contour lines drawn every 0.5 mag. middle: The Stokes *I* images with contour lines plotted in steps of 0.5 mag. bottom: The degree of linear polarization images with the polarization vectors. For comparison, the contour lines of the Stokes *I* images are overlaid. The left panels in the middle and the bottom are at *H* band. The right panels are at *K* band. top-right: A diagram to explain the important features which our images show.

Since we still only have limited knowledge of Frosty Leo, we applied simplified models to explain the bipolarity of the nebula and aspects of the grain properties. Before our experiment, we followed model calculations which were previously reported (e.g. Lopez *et al.* 2001; Dougados *et al.* 1990). We found that a single dust size grain species model can not explain both the SED curve and the degree of polarization in the nebula, and that a steep latitude density gradient is required to reproduce the distinct bipolarity of Frosty Leo, assuming a large dust grain model, which was proposed by Lopez *et al.* (2001). We used a model geometry with a latitude density gradient (Kahn & West 1985) given by

$$\rho(r, \theta) = n_0 \left(\frac{r}{R_{in}} \right)^{-\beta} (1 + \epsilon \sin^2 \theta), \quad (1)$$

where $\rho(r, \theta)$ and R_{in} are the dust density distribution and the inner radius of the dust shell, respectively. We specified different dust grain models in between lower latitudes (disk) and higher latitudes (nebula). The dust grain model is assumed to have silicate (Draine *et al.* 1985) spherical grain core with a water ice (Bertie *et al.* 1969) mantle. To simplify the treatment of the dust grains, the mean opacity with weights proportional to the size distribution function was used.

The free parameters are the optical depth in the equatorial direction τ , the inner radius R_{in} , β , ϵ and γ . We searched for parameter values to explain the SED, the total intensity images, and the polarization maps. Table 1 summarizes the model parameters, their adopted values, and ranges to be examined in our experiments.

Fig. 2 top-left compares the model SED to the observational results. The light scattered by dust dominates from the optical to the near-infrared. Because the shape of the SED curve at these wavelengths is similar to that of the central star ($T_{eff} \sim 3,800$ K), one expects a low wavelength dependency of the grain opacity. The strong peak in mid- to far-infrared is due to thermal emission from the nebula. The $25 \mu\text{m}$ flux reflects thermal emission by warm dust grains located at the inner boundary.

Fig. 2 top-right shows the dust grain opacity curves. Large dust grains in the disk are required to explain the low wavelength dependency of the opacity. On the other hand, small dust grains in the nebula are required to explain the degree of polarization.

Fig. 2 middle & bottom show the model Stokes *I* images and degree of polarization maps, respectively. The model Stokes *I* images could fairly reproduce the bipolar appearance and a flux peak (clump) in the NS bipolar lobes. The polarization maps reproduced the polarization disk.

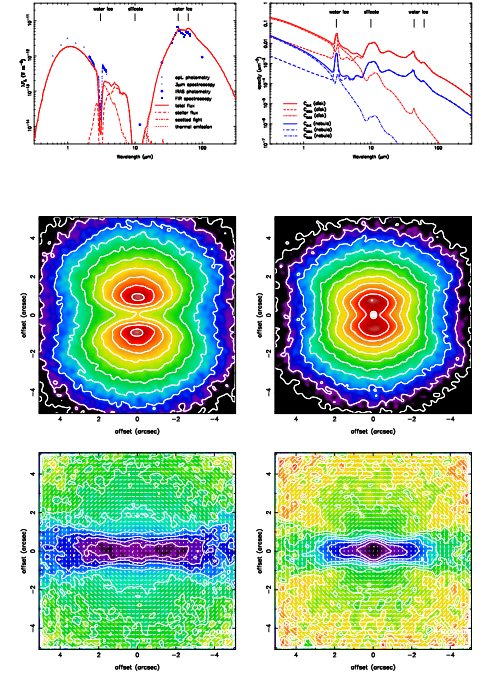


Figure 2: top-left: A comparison of the model SED. The observed SED curves are shown by the filled triangles (Rouan *et al.* 1988), the filled circles (Geballe *et al.* 1988), the filled rectangles (Omont *et al.* 1990) and the open crosses (IRAS photometry). top-right: Opacity curves of the model dust grains. The red and blue curves are for the disk and the nebula, respectively. middle & bottom: The results of our model images and polarization maps, respectively. The left panels and right panels are at *H* and *K* bands, respectively.

Parameters	Values	Range
stellar parameters		
spectral type	K7III or II	–
effective temperature	3,800 K	3,700 – 3,800 K
luminosity (L_\odot)	$450D^2 L_\odot$	scaled
dust grain chemistry		
core (spherical)	silicate	–
mantle (constant thickness)	water ice	–
dust grain (disk)		
size range	$0.1 - 2.0 \mu\text{m}$	$0.01 - 10.0 \mu\text{m}$
size distribution (power index)	-3.5	$-2.0 - -5.0$
water ice mantle	50 % in volume	30 – 70 %
dust grain (nebula)		
size range	$0.05 - 0.8 \mu\text{m}$	$0.01 - 10.0 \mu\text{m}$
size distribution (power index)	-3.5	$-2.0 - -5.0$
water ice mantle	50 % in volume	30 – 70 %
shell geometry		
optical depth	6 at $2.2 \mu\text{m}$	3 – 10
inner radius R_{in}	$4,000 R_\odot$	$3,000 - 5,700 R_\odot$
outer radius R_{out}	$57,000 R_\odot$	fixed
radial density gradient β	2	1 – 4
equator-to-polar density ratio ϵ	9	4 – 99
latitude density gradient γ	15	3 – 100

Table 1: Derived model parameters: The stellar parameters are from Mauron *et al.* 1989. The luminosity was scaled to provide a good fitting to the observed SED.

References

- Balick, B., & Frank, A. 2002, *Ann. Rev. Astron. Astrophys.* **40**, 439
 Bertie, J. E., Labbé, H. J., & Whalley, E. 1969, *J. Chem. Phys.* **50**, 4501
 Beuzit, J.-L., Thébaud, P., Perrin, G., & Rouan, D. 1994, *A&A* **291**, L1
 Dougados, C., Rouan, D., Lacombe, F., Forveille, T., & Tiphene, D. 1990, *A&A* **227**, 437
 Draine, B. T. 1985, *Astron. Astrophys. J. Suppl. Ser.* **57**, 587
 Fischer, O., Henning, Th., & Yorke, H. W. 1994, *A&A* **284**, 187
 Forveille, T., Morris, M., Omont, A., & Lique, L. 1987, *A&A* **176**, L13
 Geballe, T. R., Kim, Y. H., Knacke, R. F., & Neill, K. S. 1988, *ApJ* **326**, L65
 Kahn, F. D., & West, K. A. 1985, *MNRAS* **212**, 837
 Kwok, S. 1993, *Ann. Rev. Astron. Astrophys.* **31**, 63
 Lohmann, A. W., Weigelt, G., & Wirtzinger, B. 1983, *Appl. Opt.* **22**, 4028
 Lopez, B., Tuthill, P. G., Danchi, W. C., Monnier, J. D., & Naccolini, G. 2001, *A&A* **377**, 90
 Mauron, N., le Borgne, J.-F., & Piquette, M. 1989, *A&A* **218**, 213
 Meyer, A. W., Smith, R. G., Charney, S. B., & Pendleton, Y. J. 1998, *ApJ* **115**, 2509
 Murakawa, K., Suto, H., Oya, S., Yates, J. A., Ueta, T., & Meixner, M. 2005, *A&A* **436**, 601
 Ohnaka, K., Driebe, T., Hofmann, K.-H. *et al.* 2006, *A&A* **445**, 1015
 Omont, *et al.* 1990, *ApJ* **355**, L27
 Roddier, F., Roddier, C., Graves, J. E., & Northcott, M. J. 1995, *ApJ* **443**, 249
 Rouan, D., Omont, A., Lacombe, F., & Forveille, T. 1988, *A&A* **189**, L3
 Sahai, R., Bujarabab, V., Castro-Carrizo, A., Zijlstra, A. 2000, *A&A* **360**, L9
 Scarrott, *et al.* 1990, *MNRAS* **245**, 484
 Smith, R. G., Sellgren, K., & Tokunaga, A. 1998, *ApJ* **334**, 209
 Weigelt, G. 1977, *Opt. Comm.* **21**, 55